



OPEN ACCESS

EDITED BY

Yong Xie,
Xidian University, China

REVIEWED BY

Zhen Cui,
Xi'an University of Technology, China
Yuliang Mao,
Xiangtan University, China

*CORRESPONDENCE

M. O. Manasreh,
✉ manasreh@uark.edu

RECEIVED 20 October 2023

ACCEPTED 15 December 2023

PUBLISHED 11 January 2024

CITATION

Andharia E, Alqurashi H, Erikat I, Hamad B and Manasreh MO (2024), Effect of strain profiling on anisotropic opto-electronic properties of As_2X_3 ($X = S, Te$) monolayers from first principles.
Front. Mater. 10:1325194.
doi: 10.3389/fmats.2023.1325194

COPYRIGHT

© 2024 Andharia, Alqurashi, Erikat, Hamad and Manasreh. This is an open-access article distributed under the terms of the [Creative Commons Attribution License \(CC BY\)](https://creativecommons.org/licenses/by/4.0/). The use, distribution or reproduction in other forums is permitted, provided the original author(s) and the copyright owner(s) are credited and that the original publication in this journal is cited, in accordance with accepted academic practice. No use, distribution or reproduction is permitted which does not comply with these terms.

Effect of strain profiling on anisotropic opto-electronic properties of As_2X_3 ($X = S, Te$) monolayers from first principles

Eesha Andharia^{1,2}, Hind Alqurashi³, Ihsan Erikat⁴,
Bothina Hamad^{1,2,5} and M. O. Manasreh^{6*}

¹Department of Physics, University of Arkansas, Fayetteville, AR, United States, ²Materials Science and Engineering (MSEN), University of Arkansas, Fayetteville, AR, United States, ³Physics Department, College of Science, Al-Baha University, Alaqiq, Saudi Arabia, ⁴Department of Physics, Isra University, Amman, Jordan, ⁵Physics Department, The University of Jordan, Amman, Jordan, ⁶Department of Electrical Engineering, University of Arkansas, Fayetteville, AR, United States

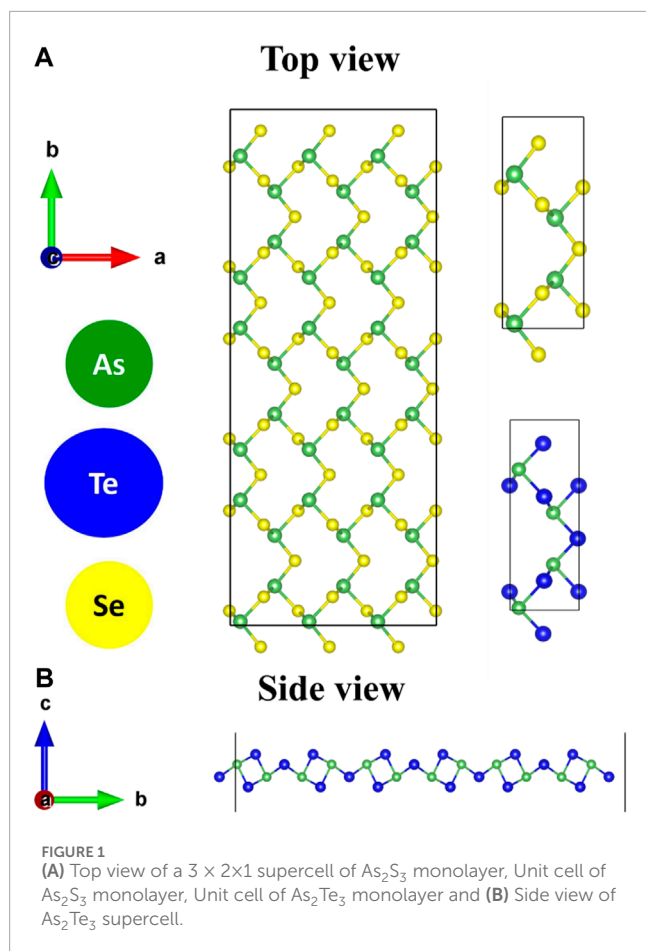
Strain Engineering is a widely adopted approach to modulate the opto-electronic performance of 2-Dimensional (2D) materials. Recently, anisotropic Van der Waals (vdW) based 2D As_2S_3 monolayer has gained significant attention within the scientific community due to its stability in ambient conditions. Similar compounds like As_2Te_3 have also been theoretically explored. However, its indirect bandgap nature limits its application in optical devices. In this study, a systematic study of compressive and tensile strain on three profiles—Uniaxial along a-axis, Uniaxial along b-axis and biaxial strain from -10% to $+10\%$, is performed for As_2S_3 and As_2Te_3 monolayers. Certain strain profiles like Uniaxial tensile strain of 8% along b-axis results in transition to direct bandgap material. Similarly, for As_2Te_3 , shear strain of $(-10\%, +8\%)$ along (a, b) axis results in direct bandgap material. In addition, the anisotropic optical absorption spectrum is obtained for unstrained and strained monolayers within the random phase approximation (RPA).

KEYWORDS

first principles, strain engineering, anisotropic van der waal's 2D materials, direct bandgap semiconductors, random phase approximation (RPA)

1 Introduction

Intrinsic in-plane structural anisotropy in vdW-based 2D materials gives rise to directionally dependent electronic, optical, magnetic, and mechanical properties that can be exploited for device physics. This class of materials known as T and T' metal dichalcogenides (TMDCs) include ReS_2 (Lin et al., 2015) and $ReSe_2$ (Wolverson et al., 2014), Phosphorene (Wang et al., 2015), Borophene (Padilha et al., 2016), transition metal monochalcogenides MX (Sarkar and Stratakis, 2020), where M = Ge, Pb, Sn and X = Se, S, P and Te. Other examples of such anisotropic 2D vdW's materials are Antimonene (Pumera and Sofer, 2017), TiS_3 (Dai and Zeng, 2015), $ZrGeTe_4$ (Adam et al., 2020), Ta_2NiS_5 (Qiao et al., 2021), and $CrOCl$ (Xu et al., 2021). Such anisotropic 2D materials find wide applications in polarization-sensitive photodetectors, optical components, and linearly polarized light sources (Yuan et al., 2015; Guo et al., 2016; Huang et al., 2019). Amongst these compounds, monolayer black phosphorus exhibits the highest anisotropic



ratio of Young's modulus along the direction of b to a axis of 2 (Tao et al., 2015; Wang et al., 2015). However, phosphorene is unstable in air (Kistanov et al., 2017), which limits its applications in devices like Nano-electro-mechanical systems (NEMS). On the other hand, a recently studied compound, namely, As_2S_3 monolayer with an in-plane anisotropic ratio of 1.7 is found to be stable under ambient conditions (Šiškins et al., 2019).

There were two independent theoretical studies carried out in 2016 (Debbichi et al., 2016; Miao et al., 2017) that predicted the possibility of the formation of few layers to monolayer As_2S_3 , As_2Se_3 and As_2Te_3 from its bulk form in naturally occurring orpiment phase. It was predicted that these materials have indirect bandgap semiconductors by using DFT and AIMD calculations (Debbichi et al., 2016; Miao et al., 2017). The anisotropic optical and mechanical properties of As_2S_3 monolayer were verified experimentally (Šiškins et al., 2019). In addition, the anisotropic thermoelectric performance of As_2S_3 and As_2Te_3 monolayers was also studied using DFT calculations (Patel et al., 2020; Gao et al., 2021). However, there is only one report on the effect of uniaxial compressive strain on the electronic properties of As_2S_3 monolayer (Liu et al., 2021a).

Mechanical deformation of two-dimensional materials is one of the most appealing methods to modify their electronic structure. By straining the interatomic distances, the bond-lengths change leading to a change in the overlap of the electronic wavefunctions of the atomic orbitals, which has an impact on the electronic structure of

these materials. For instance, the direct bandgap of phosphorene was found to change to indirect by applying biaxial strain (Peng et al., 2014).

The materials in the present work have indirect bandgaps, which limit their applications in optoelectronic devices due to unavoidable thermal dissipation due to phonon scattering. Furthermore, unlike three-dimensional materials, 2D materials can withstand a strain of up to 10% during mechanical exfoliation (Postorino et al., 2020). Hence, it is worthwhile to perform a systematic study of the effect of strain on the opto-electronic response of As_2X_3 monolayers. In this paper, we report the effect of both compressive and tensile, uniaxial, biaxial and a few cases of shear strain on the electronic and optical properties of 2D monolayer As_2X_3 ($X = \text{S}, \text{Te}$) using *ab initio* calculations. This paper is organized as follows: section- II provides the details of the calculations and computational methodology, section-III is divided in four parts—the structural and electronic properties of unstrained monolayers, the effect of uniaxial and biaxial strain on the electronic properties, a discussion of the effect of shear strain on the electronic properties and finally the effect of mechanical strain on anisotropic optical properties.

2 Computational methodology

Density functional theory calculations are performed using Vienna *ab initio* simulation package (VASP) code (Kresse and Hafner, 1993; Kresse and Furthmüller, 1996) using Projected Augmented Wave (PAW) type of pseudopotentials (Kresse and Joubert, 1999). The exchange correlation functional was treated using the generalized gradient approximation (GGA) within the Perdew–Burke–Ernzerhof (PBE) methodology (Perdew et al., 1996) by explicitly introducing the vdW interaction using optB86b functional (Klimeš et al., 2011). The cutoff kinetic energy for plane waves was set to 500 eV. 2D monolayer unit cells for both As_2S_3 and As_2Te_3 compounds were relaxed until the force convergence of 10^{-4} was achieved with an energy convergence criterion of 10^{-6} eV. The self-consistent field calculations were performed using a $8 \times 6 \times 1$ Gamma-centered k -mesh. The projected density of states (PDOS) calculations were obtained using a dense k -mesh of $30 \times 10 \times 1$. The c -axis or vacuum of 23Å was created to simulate the vdW gap to avoid the periodic repetition of the neighboring unit cells.

The linear optical properties are calculated within the random phase approximation using Kubo–Greenwood equations by calculating the microscopic dielectric constant as implemented in VASP code (Gajdoš et al., 2006). The microscopic dielectric function is given by the following Equation 1.

$$\epsilon(\omega) = \epsilon_1(\omega) + i\epsilon_2(\omega) \quad (1)$$

The imaginary part of the dielectric function that depends on transition matrix elements and joint density of states is given by Eq 2 as follows:

$$\epsilon_2(\omega) = \frac{2e^2\pi}{\Omega\epsilon_0} \sum_{k,v,c} \langle \Psi_k^c | \hat{u} \cdot r | \Psi_k^v \rangle \delta(E_k^c - E_k^v - E) \quad (2)$$

Here, ω is the frequency of the light, Ω is unit cell volume, ϵ_0 is the permittivity of free space, Ψ^c is the wavefunction of the conduction band (c) at k -point index k and Ψ^v denotes the wavefunction of the

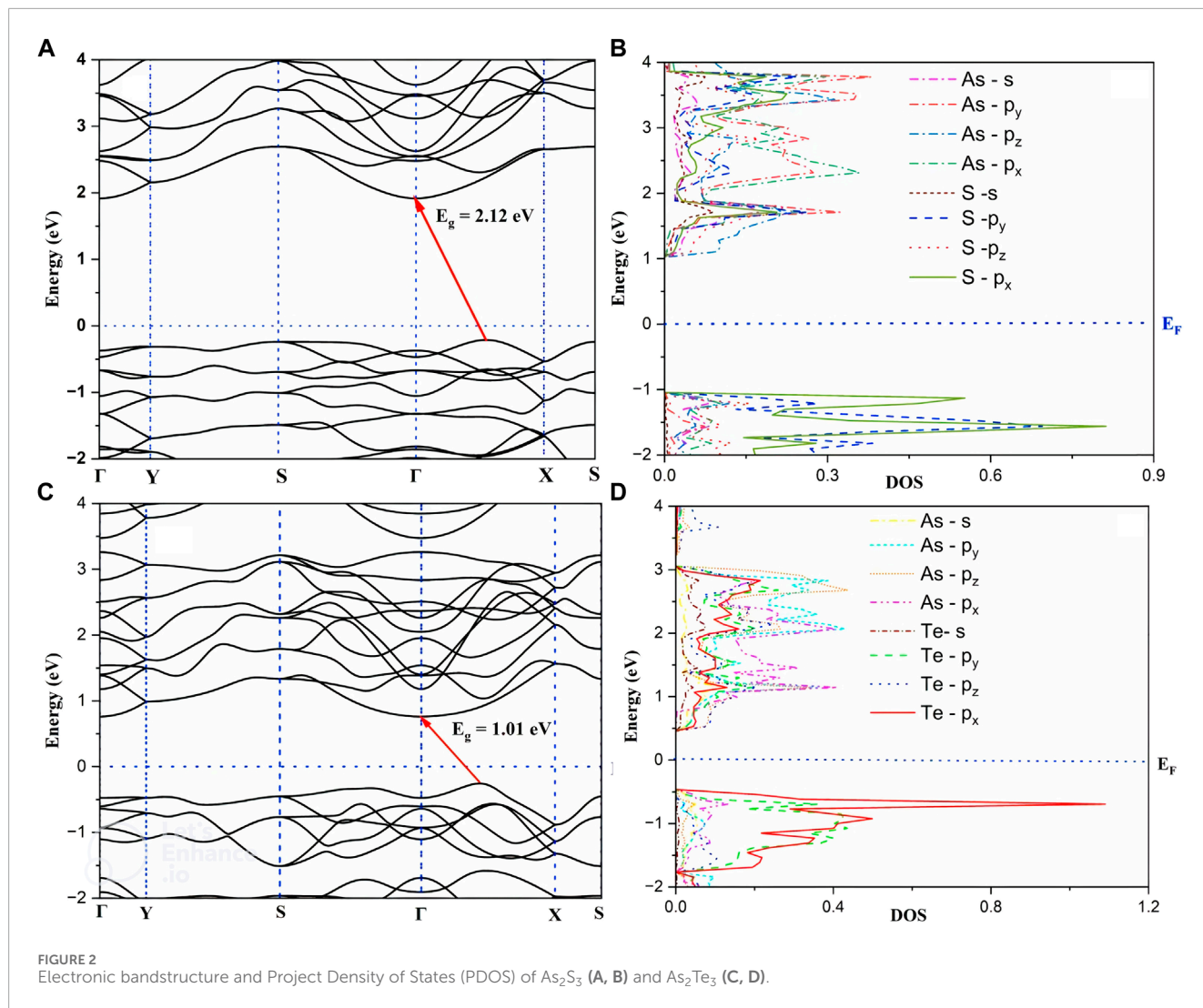


FIGURE 2 Electronic bandstructure and Project Density of States (PDOS) of As_2S_3 (A, B) and As_2Te_3 (C, D).

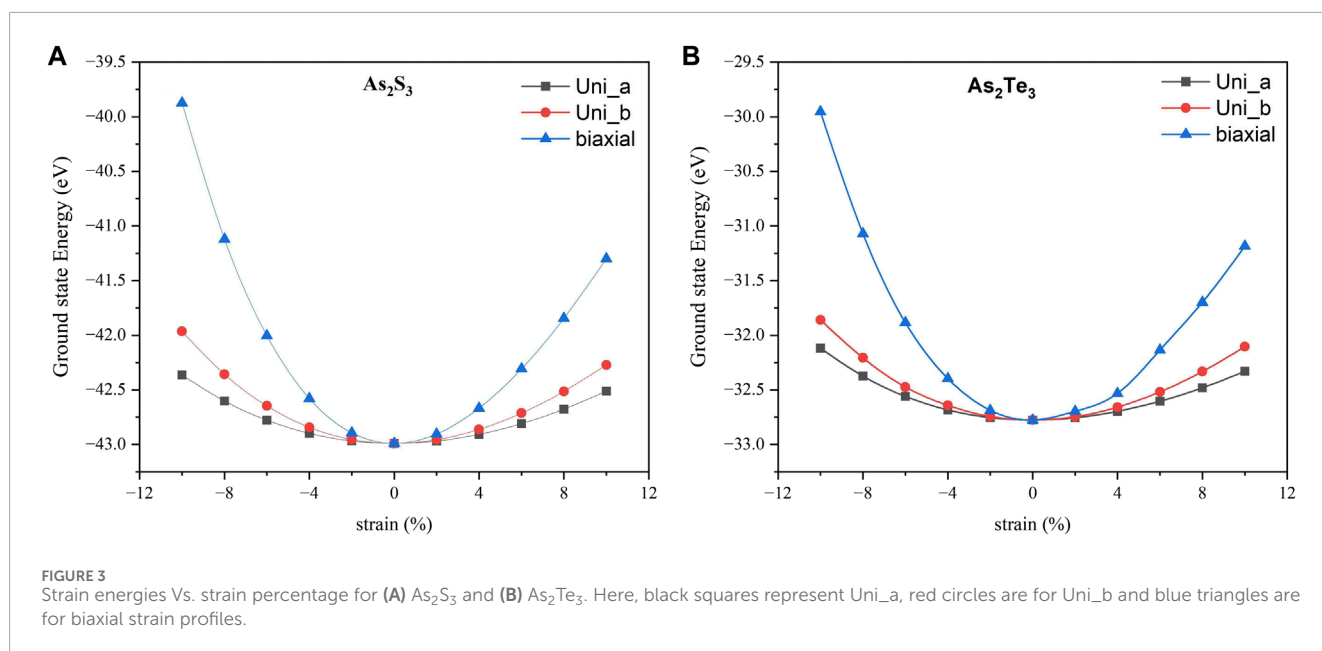
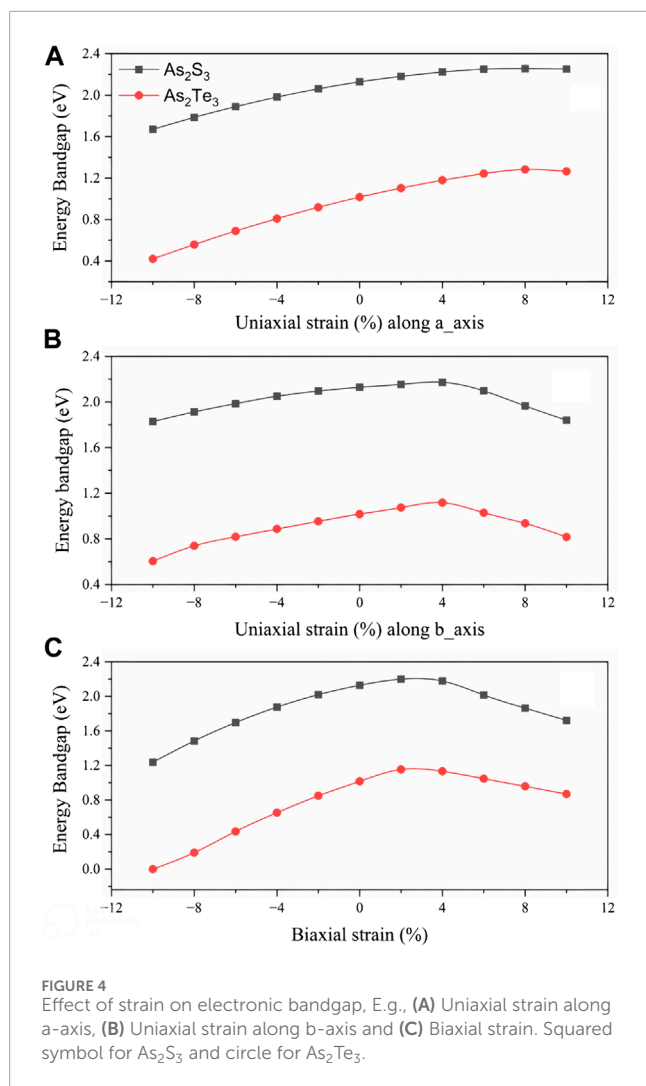


FIGURE 3 Strain energies Vs. strain percentage for (A) As_2S_3 and (B) As_2Te_3 . Here, black squares represent Uni_a, red circles are for Uni_b and blue triangles are for biaxial strain profiles.



valence bands, \hat{u} . r is the direction of polarization of incident light. The real part $\epsilon_1(\omega)$ is obtained by Kramer-Kronig transformation. The optical properties are calculated by considering the light parallel to both, a (XX)- and b (YY)-axes. A denser k-mesh of $30 \times 10 \times 1$ was used for the calculation of linear optical properties.

The strain is calculated by the relation $\epsilon = (l-l_0)/l_0$, where l is the length of the strained unit cell vector and l_0 is the unstrained unit cell vector length. Both compressive and tensile uniaxial (along a-axis and b-axis due to anisotropic unit cell) and biaxial strain were applied by varying the strain to the unit cell from -10% to $+10\%$. Moreover, the effect of shear strain for a particular case of applying the compressive strain on a-axis is studied from -2% to -10% and the b-axis was fixed to $+8\%$ tensile strain. The postprocessing is performed using VASPKIT (Wang et al., 2021).

3 Results and discussion

3.1 Structural and electronic properties of unstrained monolayers As_2X_3

Figure 1A shows a fully relaxed $3 \times 2 \times 1$ supercell of As_2S_3 monolayer. The rectangular primitive unit cells of As_2S_3 and As_2Te_3

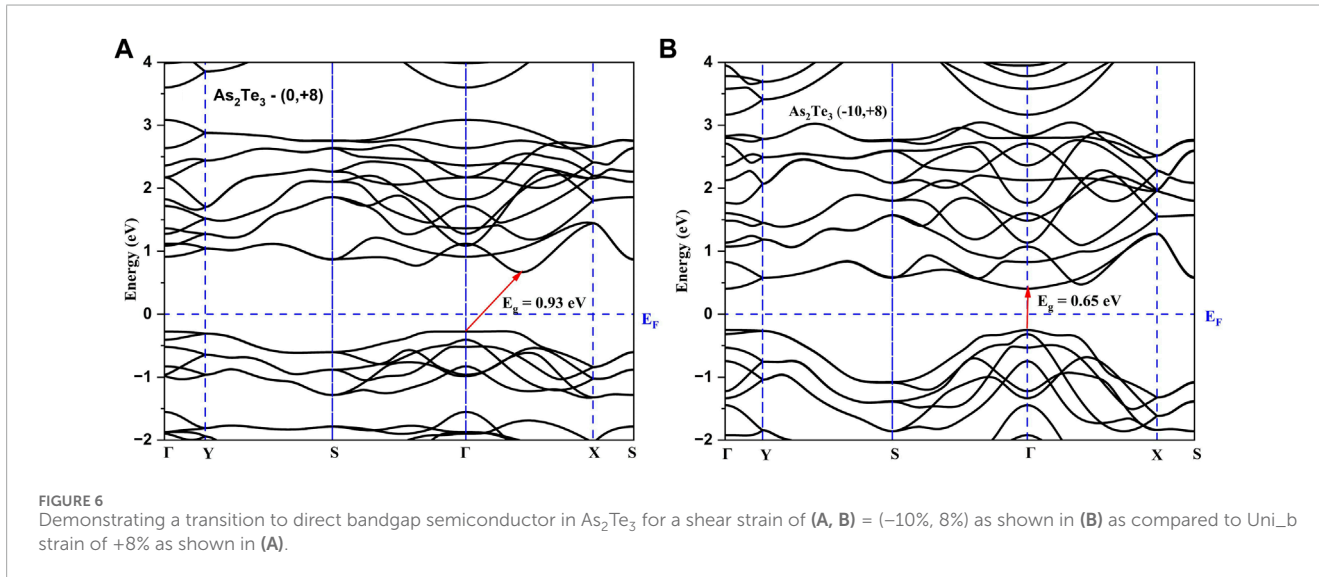
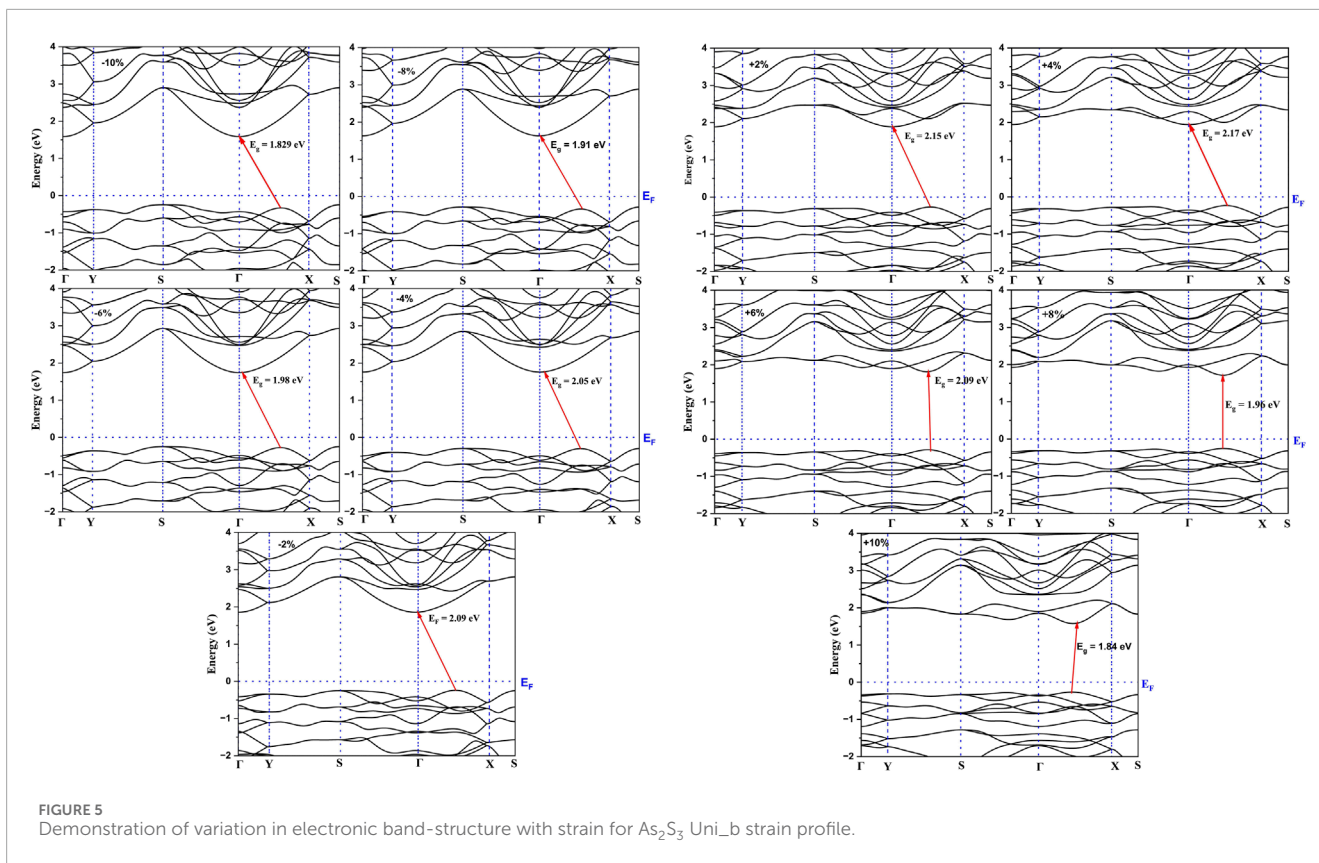
are shown in Figure 1A. They belong to the orthorhombic lattice with space group Pmn21 (Space group number 31). Each unit cell consists of two formula units of As_2X_3 . The As atoms have a coordination number of three and each S/Te atom has a coordination number of two. Figure 1B presents a side view of As_2Te_3 supercell.

The calculated lattice vectors of As_2S_3 are $a = 4.54 \text{ \AA}$ and $b = 11.35 \text{ \AA}$ are comparable with previous theoretical results ($a = 4.45 \text{ \AA}$ and $b = 11.35 \text{ \AA}$) (Mortazavi et al., 2020). However, they are higher than the experimental findings of 4.22 \AA and 11.46 \AA (Nobuo, 1954). The optimized lattice parameters of As_2Te_3 are $a = 4.56 \text{ \AA}$ and $b = 13.14 \text{ \AA}$ in this study compare well with previous theoretical results ($a = 4.45 \text{ \AA}$ $b = 13.11 \text{ \AA}$) (Mortazavi et al., 2020). In reference (Liu et al., 2021b), the theoretical lattice parameters for monolayer As_2S_3 are $a = 4.41 \text{ \AA}$ and $b = 11.41 \text{ \AA}$. In these references, the calculations are performed using Grimme's DFT-D2 input DFT functional for vdW's interactions, but in the present study, calculations are done differently using optPBE-vdW's functional as mentioned in the computational methodology. So, the lattice parameters obtained in both the calculations vary slightly. The mechanical anisotropy for As_2S_3 has been studied theoretically (Liu et al., 2021b) and verified experimentally in reference (Šiškins et al., 2019). Similar anisotropic behavior has also been theoretically reported for As_2Te_3 in references (Mortazavi et al., 2020; Gao et al., 2021). The phonon dispersions of both monolayers have already been studied in references (Patel et al., 2020) and (Gao et al., 2021), exhibiting no imaginary frequencies. Hence, both the compounds are dynamically stable.

The electronic band structure and PDOS of As_2S_3 and As_2Te_3 monolayers are shown in Figure 2. Both structures show a semiconducting behavior with indirect bandgap values of 2.12 and 1.01 eV for As_2S_3 and As_2Te_3 as shown in Figures 2A, C, respectively. The CBM is located at the Gamma-point and the VBM is located at line between the Γ and X high symmetry points in the first Brillouin zone. Since the curvature near VBM and CBM is high or the gradient of PDOS near the fermi energy level for VBM and CBM is larger, the charge carriers are highly delocalized. Figures 2B, D show PDOS for As_2S_3 and As_2Te_3 , respectively. From 2(b), As-pz orbital has maximum contribution to the conduction band near the Fermi-energy level, whereas S-px and S-py orbitals have most contribution to valence band states near Fermi level. Similarly, for As_2Te_3 , Te-px and py orbitals have maximum contribution to the formation of valence bands near EF and the conducting bands are formed mainly from As-pz orbital.

3.2 The effect of uniaxial and biaxial compressive and tensile strains on the electronic properties of As_2X_3 monolayers

In this subsection, the effect of strain on electronic properties of these monolayers is investigated in a comprehensive manner. Here, we consider compressive and tensile strain profiles of three different types: 1) Uniaxial strain along a_axis (Uni_a), 2) Uniaxial strain along b_axis (Uni_b), 3) Biaxial strain varying from -10% to $+10\%$ (compressive to tensile - biaxial). Figure 3 shows the



graph of DFT energies *versus* strain for Uni_a, Uni_b and biaxial strains for (a) As_2S_3 and (b) As_2Te_3 . It is clear from Figure 3 that the unstrained structure has a minimum or ground state, which indicates the most stable structure for both monolayers. In addition, the energy of the biaxial strain profile is always higher compared to uniaxial strain profiles. Also, the strain energies for Uni_a are consistently lower than that of Uni_b, implying that the structure undergoes maximum deformation along the a_axis. It is also important to note that the strain energies are always lower for

As_2Te_3 as compared to As_2S_3 , implying that As_2Te_3 can be deformed more easily.

The most important property for optoelectronic applications is the bandgap, E.g., Figure 4 shows the effect of strain on the bandgap of As_2S_3 and As_2Te_3 monolayers. In this work, the effect of strain is studied in the range from -10% to +10% (with increasing bond length from -10% to +10% strain) as shown in Figure 4A, where the bandgap is maximized at Uni_a tensile strain of +8% for both As_2S_3 and As_2Te_3 monolayers. However, the

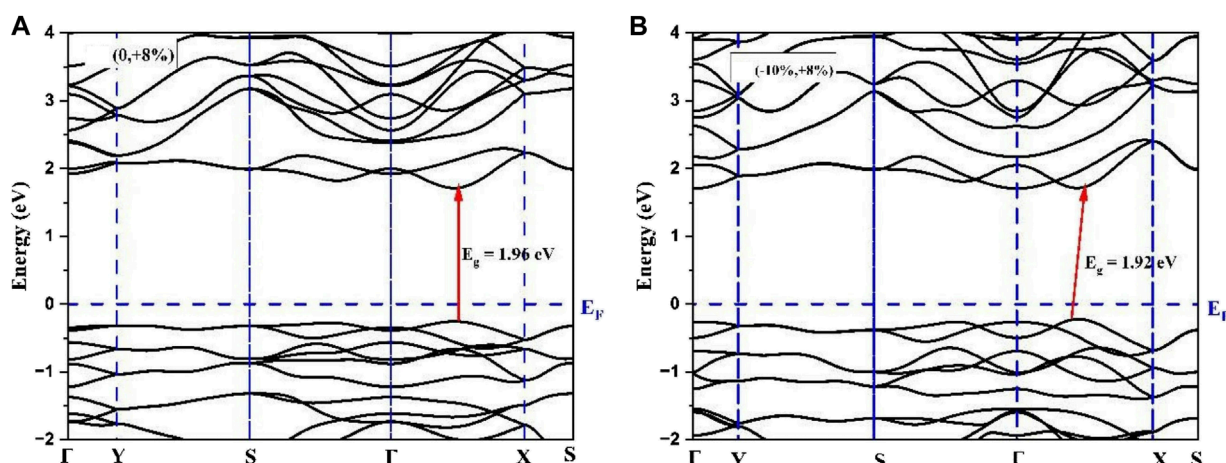


FIGURE 7 Demonstrating the loss of direct band gap nature from (A) (0, +8%) to (B) (-10%, +8%) in As_2S_3 monolayer.

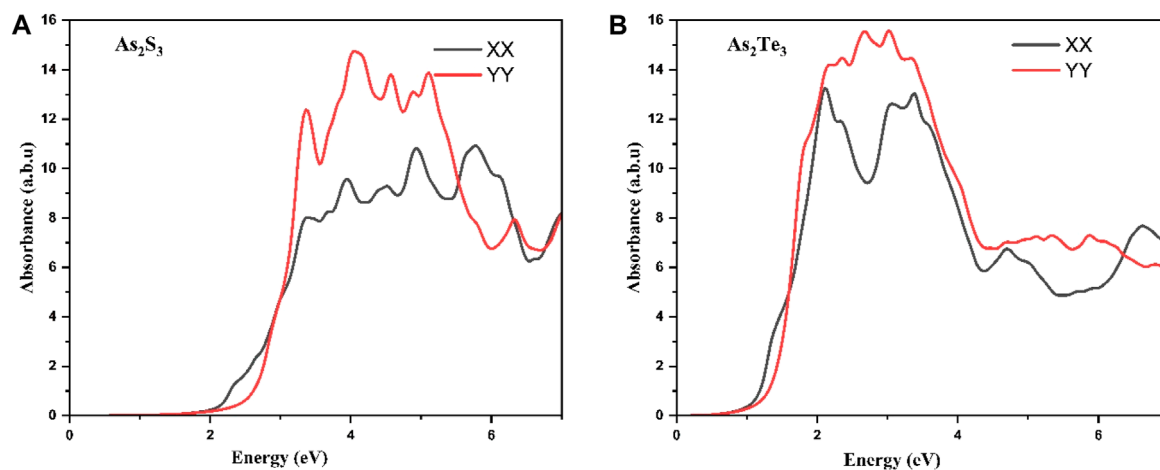


FIGURE 8 Optical absorption spectra for unstrained (A) As_2S_3 and (B) As_2Te_3 monolayers exhibiting anisotropic dependence along XX and YY direction.

bandgap maxima of As_2S_3 and As_2Te_3 monolayers are located at +4% and +2% for Uni_b tensile strain and biaxial tensile strain, respectively, see Figures 4B, C. A single example for Uni_b As_2S_3 case is considered in this study to understand this trend of the band structure changes (see Figure 5). As evident from Figure 5, the CBM shifts from Γ -point towards X-point, with increasing strain from -10% to +10%. This trend can be explained using the projected density of states for all strain profiles varying from -10% to +10%, see Supplementary Figures S1A–J. As evident from the Supplementary Figures S1A–C, for strain profiles -10%, -8% and -6%, the major contribution to CBM comes from As-*py*, As-*pz* and S-*pz* orbitals. On further reducing the compressive strain percentage for -4% and -2%, S-*py* orbital also contributes to CBM. Further going from the unstrained profile of 0% to +10%, As-*px* orbital also makes a significant contribution to CBM states near the Fermi energy level and it increases with increasing tensile strain. However, as we go from +2% to +10%, the contributions from As-*py* and S-*pz* orbitals cease to exist, see

Supplementary Figures S1E–J. This results in the shift of CBM from Γ -point towards X-point.

There is a transition from indirect to direct bandgap in As_2S_3 for uniaxial strain of 8% along b-axis (See the electronic band structure in Figure 5, whereas it retains its indirect nature for all the other strain profiles. Although, it seems that for +6% and +10%, the CBM and VBM are located closely along the Γ -X line, they are still indirect. Moreover, the system becomes metallic for the case of As_2Te_3 at biaxial compressive strain of -10% (Supplementary Figure S2) but is indirect semiconducting in all other strain profiles.

3.3 The effect of shear strain on the electronic properties of As_2X_3 monolayers

The employed strategy for selecting a limited number of shear strain profiles was as follows: Since the uniaxial strain along b-axis (Uni_b) resulted in a transition to direct bandgap semiconductor in

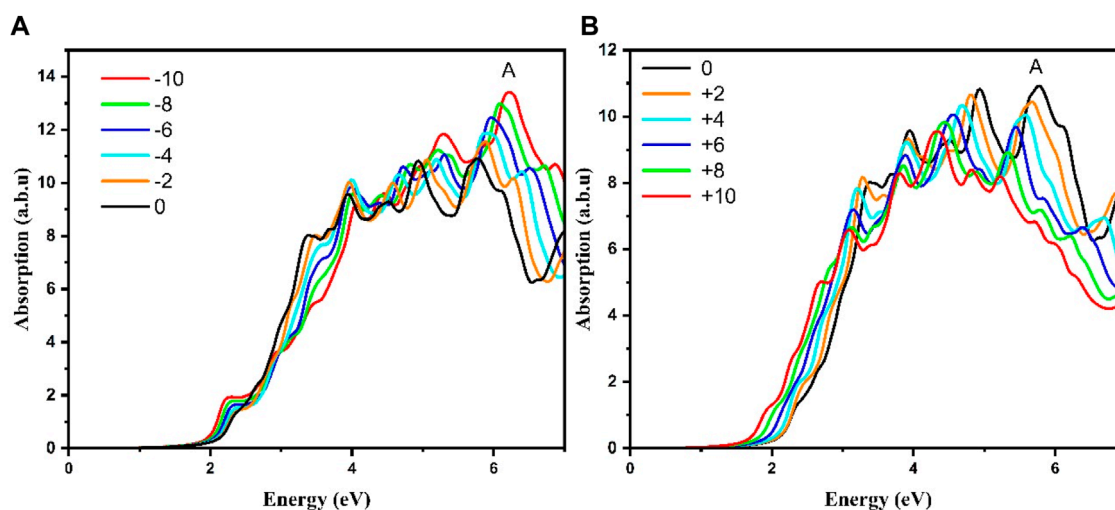


FIGURE 9 Effect of strain on optical absorption spectrum of (A) compressive strain and (B) tensile strain for Uni_b As₂S₃ monolayer.

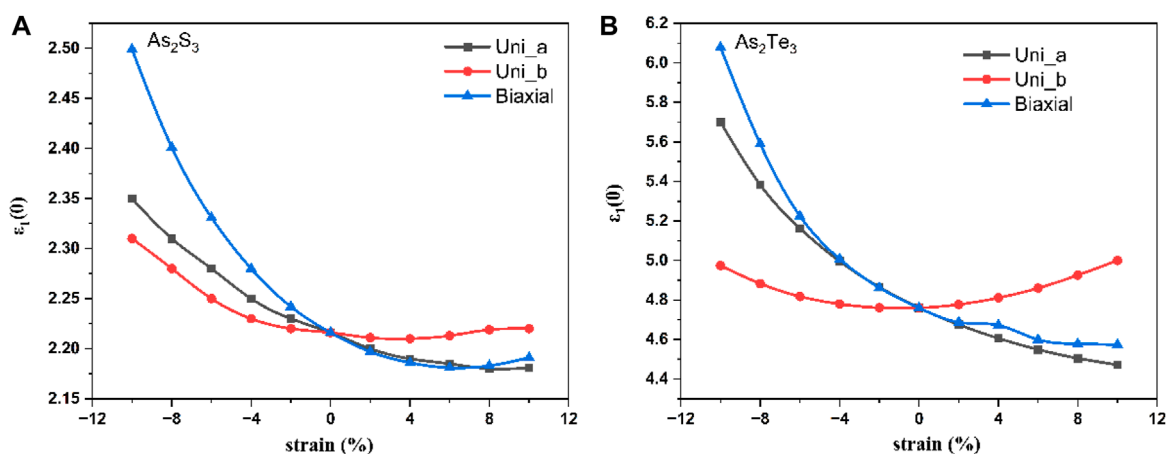


FIGURE 10 Static dielectric constant Vs. strain for monolayer As₂S₃ (A) and As₂Te₃ (B).

As₂S₃ at +8%, it is kept fixed at this b-axis tensile strain, whereas that along the a-axis was varied from -2% to -10% for both compounds. As a result, As₂Te₃ transformed to a direct band gap material, whereas, As₂S₃ lost its direct bandgap nature. As indicated in Figures 6, 7 the comparative effect of shear strain in As₂Te₃ and As₂S₃ is shown for two cases: (0%, +8%) and (-10%, 8%), respectively.

3.4 Optical properties

In this section, the anisotropy in the optical absorption spectrum is discussed in the case of unstrained As₂S₃ and As₂Te₃ monolayers. As shown in Figures 8A, B, there is a strong anisotropic behavior as demonstrated in the absorption along XX and YY-direction. For

the case of As₂S₃, there is a strong absorption in the UV range in the XX direction, which spans to some part of VIS spectrum along the YY direction, the absorption peak is in the mid to near UV range and green, blue, violet and cyan parts of VIS spectrum. Similarly, for As₂Te₃ the absorption along both directions is in the near-IR, VIS and near-UV range. The optical bandgap can be calculated by drawing a tangential line to the absorption edge along XX direction, because the band gap is along the Γ -X line in the first Brillouin zone. Figures 8A, B show that the optical, e.g., for As₂S₃ and As₂Te₃ are 1.98 and 0.88 eV, respectively.

The next step was devoted to study the effect of strain on the band gap. Here only the case of strained As₂S₃ monolayer along Uni_b (Uniaxial b-axis) is considered, since there was a transition to a direct bandgap behavior at +8% tensile strain as

depicted in Figures 9A, B. It is also important to note that only the XX-direction is considered since the bandgap is located along the Γ -X line. The absorption band-edge is red shifted along with increasing compressive strain from 0% to -10% and is again red shifted for increasing tensile strain from 0 to +10%.

The other important quantity is the static dielectric constant $\epsilon_1(0)$ and the effect of strain on it as shown in Figure 10A for As_2S_3 and Figure 10B for As_2Te_3 . This is because it has the following relation with the bandgap:

$$\epsilon_1(0) = 1 + \left(\frac{\hbar\omega_p}{2\pi * E_g} \right)^2 \quad (3)$$

Hence, it can be said that opposite trends of decreasing bandgaps with increasing $\epsilon_1(0)$ should be observed. For all the three types of strain - Uni_a, Uni_b and biaxial strain, the minima occur at +8% tensile strain whereas, for As_2Te_3 minima occurs at 0% strain for Uni_b, however, it does not reach a minimum value for Uni_a and Biaxial strain. This shows that the plasma frequency plays an important role in all the above cases.

4 Conclusion

The effect of strain profiling on the optoelectronic performance of As_2X_3 monolayers is studied. One can expect a quantifiable increase in the, E.g., values on considering the above computationally extensive calculations like the use of hybrid functionals or GW-method implementation. The strain effect on the electronic and optical properties of As_2X_3 ($X = \text{S}, \text{Te}$) monolayers is investigated and presented. It was observed that for both monolayers, E.g., has maxima for at 8%, 4%, and 2% for uniaxial a-axis, uniaxial b-axis and biaxial strain profiles, respectively. There is a direct effect of strain on red shifting or blue shifting of the absorption spectrum depending on the material and strain profiling.

5 Scope statement

I am submitting the attached paper entitled "Effect of Strain Profiling on Anisotropic Opto-Electronic Properties of As_2X_3 ($X = \text{S}, \text{Te}$) Monolayers from First Principles," by Andharia, et al. for your consideration of publishing it in *Frontiers in Materials*, section semiconductor materials and device. In this paper, we report on the effect of strain profiling on the optoelectronic performance of As_2X_3 monolayers. The band gap (E.g.,) values of these 2D materials were obtained by computationally extensive calculations. The strain effect on the electronic and optical properties of As_2X_3 ($X = \text{S}, \text{Te}$) monolayers is investigated and presented in this paper. It was observed that for both monolayers, E.g., has maxima for at 8%, 4%, and 2% for uniaxial a-axis, uniaxial b-axis and biaxial strain profiles, respectively. There is a direct effect of strain on red shifting or blue shifting of the absorption spectrum depending on the material and strain profiling. We believe this paper is very useful for the research community and we would like for you to give it a full consideration in publishing it in your journal.

Data availability statement

The raw data supporting the conclusion of this article will be made available by the authors, without undue reservation.

Author contributions

EA: Investigation, Methodology, Writing-original draft. HA: Investigation, Methodology, Software, Writing-review and editing. IE: Investigation, Methodology, Software, Writing-review and editing. BH: Investigation, Software, Supervision, Writing-review and editing. OM: Investigation, Supervision, Writing-review and editing.

Funding

The author(s) declare financial support was received for the research, authorship, and/or publication of this article. BH is supported by the MonArk Quantum Foundry that is funded by the National Science Foundation Q-AMASE-i program under NSF Award No. DMR-1906383.

Acknowledgments

The authors would like to thank Arkansas High Performance Computing Center (AHPCC), University of Arkansas, for the computing resources.

Conflict of interest

The authors declare that the research was conducted in the absence of any commercial or financial relationships that could be construed as a potential conflict of interest.

The author(s) declared that they were an editorial board member of *Frontiers*, at the time of submission. This had no impact on the peer review process and the final decision.

Publisher's note

All claims expressed in this article are solely those of the authors and do not necessarily represent those of their affiliated organizations, or those of the publisher, the editors and the reviewers. Any product that may be evaluated in this article, or claim that may be made by its manufacturer, is not guaranteed or endorsed by the publisher.

Supplementary material

The Supplementary Material for this article can be found online at: <https://www.frontiersin.org/articles/10.3389/fmats.2023.1325194/full#supplementary-material>

References

- Adam, M. L., Moses, O. A., Rehman, Z. u., Liu, Z., Song, L., and Wu, X. (2020). Band gap engineering of monolayer zrte_2 via strain: a first-principles study. *Mater. Chem. Phys.* 253, 123308. doi:10.1016/j.matchemphys.2020.123308
- Dai, J., and Zeng, X. C. (2015). Titanium trisulfide monolayer: theoretical prediction of a new direct-gap semiconductor with high and anisotropic carrier mobility. *Angew. Chem. Int. Ed.* 54, 7572–7576. doi:10.1002/anie.201502107
- Debbichi, L., Kim, H., Björkman, T., Eriksson, O., and Lebegue, S. (2016). First-principles investigation of two-dimensional trichalcogenide and sesquichalcogenide monolayers. *Phys. Rev. B* 93, 245307. doi:10.1103/PhysRevB.93.245307
- Gajdoš, M., Hummer, K., Kresse, G., Furthmüller, J., and Bechstedt, F. (2006). Linear optical properties in the projector-augmented wave methodology. *Phys. Rev. B* 73, 045112. doi:10.1103/physrevb.73.045112
- Gao, Z., Zhu, T., Sun, K., and Wang, J.-S. (2021). Highly anisotropic thermoelectric properties of two-dimensional As_2Te_3 . *ACS Appl. Electron. Mater.* 3, 1610–1620. doi:10.1021/acsaem.0c01100
- Guo, Q., Pospischil, A., Bhuiyan, M., Jiang, H., Tian, H., Farmer, D., et al. (2016). Black phosphorus mid-infrared photodetectors with high gain. *Nano Lett.* 16, 4648–4655. doi:10.1021/acs.nanolett.6b01977
- Huang, Y., Ning, J., Chen, H., Xu, Y., Wang, X., Ge, X., et al. (2019). Mid-infrared black phosphorus surface-emitting laser with an open microcavity. *ACS Photonics* 6, 1581–1586. doi:10.1021/acsp Photonics.9b00096
- Kistanov, A. A., Cai, Y., Zhou, K., Dmitriev, S. V., and Zhang, Y.-W. (2017). The role of h_2o and o_2 molecules and phosphorus vacancies in the structure instability of phosphorene. *2D Materials* 4, 015010. doi:10.1088/2053-1583/4/1/015010
- Klimeš, J., Bowler, D. R., and Michaelides, A. (2011). Van der waals density functionals applied to solids. *Phys. Rev. B* 83, 195131. doi:10.1103/physrevb.83.195131
- Kresse, G., and Furthmüller, J. (1996). Efficient iterative schemes for *ab initio* total-energy calculations using a plane-wave basis set. *Phys. Rev. B* 54, 11169–11186. doi:10.1103/physrevb.54.11169
- Kresse, G., and Hafner, J. (1993). *Ab initio* molecular dynamics for liquid metals. *Phys. Rev. B* 47, 558–561. doi:10.1103/PhysRevB.47.558
- Kresse, G., and Joubert, D. (1999). From ultrasoft pseudopotentials to the projector augmented-wave method. *Phys. Rev. B* 59, 1758–1775. doi:10.1103/physrevb.59.1758
- Lin, Y.-C., Komsa, H.-P., Yeh, C.-H., Björkman, T., Liang, Z.-Y., Ho, C.-H., et al. (2015). Single-layer re_2 : two-dimensional semiconductor with tunable in-plane anisotropy. *ACS Nano* 9, 11249–11257. doi:10.1021/acsnano.5b04851
- Liu, X., Lv, B., Ding, Z., and Luo, Z. (2021a). External uniaxial compressive strain induced built-in electric field in bilayer two-dimensional As_2S_3 for photocatalytic water splitting: a first-principles study. *Appl. Surf. Sci.* 535, 147701. doi:10.1016/j.apsusc.2020.147701
- Liu, X., Zhang, Z., Ding, Z., Lv, B., Luo, Z., Wang, J.-S., et al. (2021b). Highly anisotropic electronic and mechanical properties of monolayer and bilayer As_2S_3 . *Appl. Surf. Sci.* 542, 148665. doi:10.1016/j.apsusc.2020.148665
- Miao, N., Zhou, J., Sa, B., Xu, B., and Sun, Z. (2017). Few-layer arsenic trichalcogenides: emerging two-dimensional semiconductors with tunable indirect-direct band-gaps. *J. Alloys Compd.* 699, 554–560. doi:10.1016/j.jallcom.2016.12.351
- Mortazavi, B., Shojaei, F., Azizi, M., Rabczuk, T., and Zhuang, X. (2020). As_2S_3 , As_2Se_3 and As_2Te_3 nanosheets: superstretchable semiconductors with anisotropic carrier mobilities and optical properties. *J. Mater. Chem. C* 8, 2400–2410. doi:10.1039/C9TC05904K
- Nobuo, M. (1954). The crystal structure of orpiment (As_2S_3) refined. *Mineralogical J.* 1, 160–169. doi:10.2465/minerj1953.1.160
- Padilha, J. E., Miwa, R. H., and Fazzio, A. (2016). Directional dependence of the electronic and transport properties of 2d borophene and borophane. *Phys. Chem. Chem. Phys.* 18, 25491–25496. doi:10.1039/C6CP05092A
- Patel, A., Singh, D., Sonvane, Y., Thakor, P. B., and Ahuja, R. (2020). Bulk and monolayer As_2S_3 as promising thermoelectric material with high conversion performance. *Comput. Mater. Sci.* 183, 109913. doi:10.1016/j.commatsci.2020.109913
- Peng, X., Wei, Q., and Copple, A. (2014). Strain-engineered direct-indirect band gap transition and its mechanism in two-dimensional phosphorene. *Phys. Rev. B* 90, 085402. doi:10.1103/physrevb.90.085402
- Perdew, J. P., Burke, K., and Ernzerhof, M. (1996). Generalized gradient approximation made simple. *Phys. Rev. Lett.* 77, 3865–3868. doi:10.1103/physrevlett.77.3865
- Postorino, S., Grassano, D., D'Alessandro, M., Pianetti, A., Pulci, O., and Palumbo, M. (2020). Strain-induced effects on the electronic properties of 2d materials. *Nanotechnol.* 10, 184798042090256. doi:10.1177/1847980420902569
- Pumera, M., and Sofer, Z. (2017). 2d mono-elemental arsenene, antimonene, and bismuthene: beyond black phosphorus. *Adv. Mater.* 29, 1605299. doi:10.1002/adma.201605299
- Qiao, J., Feng, F., Wang, Z., Shen, M., Zhang, G., Yuan, X., et al. (2021). Highly in-plane anisotropic two-dimensional ternary ta_2nise_5 for polarization-sensitive photodetectors. *ACS Appl. Mater. Interfaces* 13, 17948–17956. doi:10.1021/acsmi.1c00268
- Sarkar, A. S., and Stratakis, E. (2020). Recent advances in 2d metal monochalcogenides. *Adv. Sci.* 7, 2001655. doi:10.1002/advs.202001655
- Šiškins, M., Lee, M., Aljani, F., van Blankenstein, M. R., Davidovikj, D., van der Zant, H. S. J., et al. (2019). Highly anisotropic mechanical and optical properties of 2d layered As_2S_3 membranes. *ACS Nano* 13, 10845–10851. doi:10.1021/acsnano.9b06161
- Tao, J., Shen, W., Wu, S., Liu, L., Feng, Z., Wang, C., et al. (2015). Mechanical and electrical anisotropy of few-layer black phosphorus. *ACS Nano* 9, 11362–11370. doi:10.1021/acsnano.5b05151
- Wang, L., Kutana, A., Zou, X., and Jakobson, B. I. (2015). Electro-mechanical anisotropy of phosphorene. *Nanoscale* 7, 9746–9751. doi:10.1039/C5NR00355E
- Wang, V., Xu, N., Liu, J.-C., Tang, G., and Geng, W.-T. (2021). Vaspkit: a user-friendly interface facilitating high-throughput computing and analysis using vasp code. *Comput. Phys. Commun.* 267, 108033. doi:10.1016/j.cpc.2021.108033
- Wolverson, D., Crampin, S., Kazemi, A. S., Ilie, A., and Bending, S. J. (2014). Raman spectra of monolayer, few-layer, and bulk re_2 : an anisotropic layered semiconductor. *ACS Nano* 8, 11154–11164. doi:10.1021/nn5053926
- Xu, C., Zhang, J., Guo, Z., Zhang, S., Yuan, X., and Wang, L. (2021). A first-principles study on the electronic property and magnetic anisotropy of ferromagnetic cro and crocl monolayers. *J. Phys. Condens. Matter* 33, 195804. doi:10.1088/1361-648X/abe477
- Yuan, H., Liu, X., Afshinmanesh, F., Li, W., Xu, G., Sun, J., et al. (2015). Polarization-sensitive broadband photodetector using a black phosphorus vertical p–n junction. *Nat. Nanotechnol.* 10, 707–713. doi:10.1038/nnano.2015.112